

Dynamic Study of A Wind Turbine Blade Using Bond Graph

Zakaria Khaouch¹, Mustapha Zekraoui¹, Mustapha Adar¹,
Nourreedine Kouider¹, Mustapha Mabrouki¹

¹*Industrial Engineering Laboratory, Faculty of Science and Technology, Sultan Moulay Slimane University,
Beni Mellal, Morocco.*

Corresponding Author: Zakaria Khaouch

Abstract: *The design of a wind turbine system (sizing, control), needs the use of performing simulation tools agreeing to specifications in terms of quality of produced electricity, stability and safety. The effects of the wind speed change, the variation of cinematic movement parameters, the structure aero elastic response and the definition of subsystems characteristics that makes the entire wind turbine system, including blades, tower, drive train, rotor and control system allow one to characterize the structural dynamic behavior of the wind turbine. This paper presents a novel methodology to study the dynamic behavior of wind turbine blades with horizontal axis using the Bond Graph Method. The model is based on the theory of three-dimensional Rayleigh beam, composed of a number of variable sections of the type NACA 4415 airfoil, and takes into account the axial and tangential flexion and free torsion effects with regards to the aerodynamic loads (the lift, the drag and the pitching moment) calculated using the BEM theory. A validation has been undertaken by considering data from a NACA 4415 blade profile.*

Keywords: *Aerodynamic, BEM theory, Bond Graph, wind turbine blade*

Date of Submission: 07 -11-2017

Date of acceptance: 30-11-2017

I. Introduction

Energy is an essential element for the economic progress of most countries. The increasing concern about climate change and pollution has led to the development and improvement of renewable energy sources. Wind energy is the fastest-rising renewable source. The most common device to convert the wind kinetic energy into electrical power is the horizontal axis wind turbine (HAWT), typically having a three-blade rotor. The power captured by wind turbines is proportional to the swept area of the rotor disc, to be a competitive energy resource over other energy generation systems, the overall wind turbines size (blades) must be increased. At the same time, the turbine weight must be less. This results in more slender and lighter structure. Therefore, the aero elastic deformation of wind turbines structure (blades) is unavoidable, which leads to vibratory loads, and alters the turbine power performance [1]. Consequently, it is important to better understand the aero elastic behaviors of the rotor blades such that large-scale wind turbines well be designed to be a more efficient and reliable energy production system.

There have been many studies on the blade dynamic problem, [1] established a three-degrees-of-freedom analytical model (including rigid body flap, lead/lag and feather motion) for a rigid blade and studied the nonlinear dynamics of the blade. [2] considered horizontal axis wind turbine as a multi-flexible-system composed of rigid subsystems (hub and nacelle) and flexible subsystems (blade and tower). And established a blade model by using the FEM. [3] use the principle of virtual work in combination with the FEM to model the wind turbine blade in which the warping, extension and tilt effects of the cross section were included. [4-7] introduced a variational model for the coupled flap-lead/lag-feather vibration of blades based on the Euler-Bernoulli beam theory. The effect of support point motion was emphasized in this model. [8] proposed an analytical model for the couple extension-flap-lead/lag-feather vibration of elastic, isotropic, non-uniform blades, and dealt with linear modal and nonlinear normal modes problems. [9] introduced a mathematical model for the lead/lag motion of a blade subjected to gravitational and aerodynamic loading, and performed a perturbation analysis for the nonlinear dynamics of the blade in super- and sub-harmonic resonances.

These works on analytical models of rotating blades are all dealing with only structural part or aerodynamic part. Therefore, it is necessary to move towards a more unified approach for modelling wind turbine systems as a whole for understanding, analyzing and hence designing this multidisciplinary system [10]. Bond graph methodology allows its further integration to bond graph model of drive train, tower and generator providing a common platform to access the whole turbine system [10] and to deal with control problems [11].

A Bond Graph [10,11,12,13] is a graphical representation of a physical dynamic system. It is similar to the better known block diagram and signal-flow graph, with the major difference that the arcs in bond graphs represent bi-directional exchange of physical energy, while those in block diagrams and signal-flow graphs represent unidirectional flow of information. In addition, Bond Graphs are multi-energy domain (e.g. mechanical, electrical, hydraulic, etc.). This means that a Bond Graph can incorporate multiple domains seamlessly.

The Bond Graph is composed of the "bonds" which link together "single port", "double port" and "multi-port" elements (R , I , C , TF and GY) [10,11,12,13]. Each bond represents the instantaneous flow of energy ($dE(t)/dt$) or power $P(t)$. A pair of variables called "power variables" whose product is the instantaneous power of the bond denotes the flow of energy in each bond. Each domain's power variables are broken into two types: "effort $e(t)$ " and "flow $f(t)$ ". Effort multiplied by flow produces power, thus the term power variables. Every domain has a pair of power variables with corresponding effort and flow variables.

Causality - a bond graph must determine which of the two power signals for the subsystem is entering, and which in turn dependent variable, thus acting on the subsystem. Causality is referred by perpendicular to the detention site where the flow enters the subsystem variable effort. Between the building elements of bond graphs which in practice are sufficient, and that we classify according to the number of bonds are one-port, two-port and multiport. One-ports are elements that exchange energy in the system only via one link. This group includes:

- Source of effort "SE".
- Source of flow "SF".
- One port C element (Capacitor).
- One port I element (Inductor).
- One port R element (Resistor).

Two-ports are elements of the system which can exchange energy via two bonds. Thus, two-ports retain power, it is supposed that the product of effort and flow at the exit is equal to the product of effort and flow at the inlet. There are two basic types of two-ports:

- Transformer "TF".
- Gyration "GY".

One-ports are attached to two-ports in the bond graph by connecting nodes. The power is branched in the nodes. There are two types of nodes:

- 1 – junction.
- 0 – junction.

The 1 – junction for all the power bonds that lead to the same node flow (f) and node describes the balance of effort (e).

0 - junction is the power of all bonds that lead to the same node of effort (e) and node describes the balance of the flow (f).

The main advantages of the Bond Graph tool for modeling purposes are summarized through few keywords:

1. Modeling: the Bond Graph is a unified representation language, which explicitly highlights the power flows, makes possible the energetic study, simplifies models building for multi-disciplinary systems, explicitly shows up the cause - effect relations (causality) and leads to a systematic writing of mathematical models (linear or nonlinear associated).
2. Identification: identification of unknown parameters, but knowledge of the associated physical phenomena and mastering physical meaning of the obtained model.
3. Analysis: Putting to the fore the causality problems, and therefore the numerical problems, model dynamic estimation and identification of the slow and fast variables.
4. Control: Design of control laws from simplified models.
5. Simulation: Specific software (20-Sim)

In the present work, we study the dynamic structural behavior of the wind blade in term of the Bond Graph approach. The blade is considered as a three-dimensional Rayleigh beam composed of a number of sections submitted to aerodynamic forces calculated using the BEM theory. In [14], a structural model of the wind turbine blade is proposed using the bond graph approach based upon the Rayleigh beam model. The blade – assumed as a twisted beam – is divided into three components, each of which is subject to the aerodynamic wind forces. Nevertheless, the deformation of the axial extension and the pitching moment applied to the center of gravity are not taken into consideration. These "gaps" are addressed in this paper where they are integrated in our model. The model describe the nonlinear vibration of wind turbine blades. The system consists of three components of deformation including longitudinal vibration (named axial extension), outof-plane bend (named flap), in-plane/edgewise bend (named lead/lag) and torsion (named feather).

This paper is organized as follows: Section 2 presents a Bond graph model of the wind turbine blade. Section 3 is concerned with Aerodynamic model of the wind turbine. The Section 4 includes a simulation and a validation of the proposed model. The concluding remarks are given in Section 5.

II. Bond Graph Model Of The Wind Turbine Blade

In this section, we study the structural dynamic behavior of the wind blade. A blade Bond Graph model is developed. It consists of considering the blade as a three-dimensional beam composed of a number of variable sections according to NACA 4415 aerofoil sections (Fig. 1(a)).

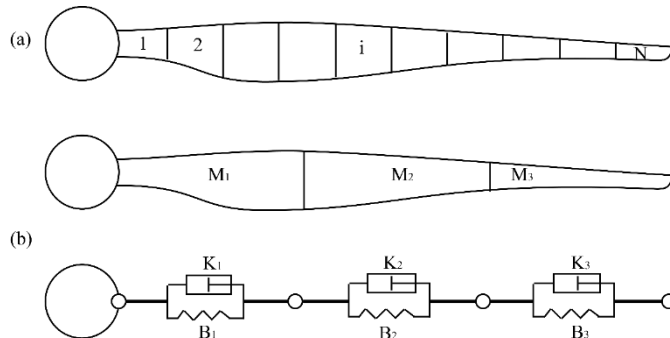


Fig. 1 Turbine Blade with space reticulation (a), Dynamic model of blade (b)

The study of the dynamic behavior of a wind turbine blade can be undertaken by various methods of analysis. The Euler-Bernoulli beam model is the simplest form. It does not consider rotary inertia of the beam and its shear deformation. However, this approximation gives nearly accurate results for slender beams, i.e., when the depth of the beam is much smaller than its length. The Rayleigh beam formulation, which accounts for the rotary inertia of the beam, is an improvement over Euler-Bernoulli formulation. Rayleigh beam formulation gives better approximation of the natural frequencies of a slender beam than the Euler-Bernoulli formulation and it requires less number of discrete elements to create a model. The shear deformation effect becomes prominent when the beam thickness is large and the model of such system is constructed by accounting for the additional deformation of each element due to the shear force. In the present work. The blade is considered as a three-dimensional Rayleigh beam composed of a number of sections submitted to aerodynamic forces. The dynamic model of the blade is shown in Fig. 1(b).

2.1. Rayleigh Beam Model

The Rayleigh beam formulation is based on shear force and bending moment representations given in Newtonian convention, where a common reference is taken for both faces of the beam element: upward shear force is positive force and anticlockwise moment is positive moment (Fig. 2). The rotation of the beam segment is explicitly modeled in Rayleigh beam formulation. The beam segment is assumed to store potential energy due to four distinct displacements: displacements of either end and rotations of either end.

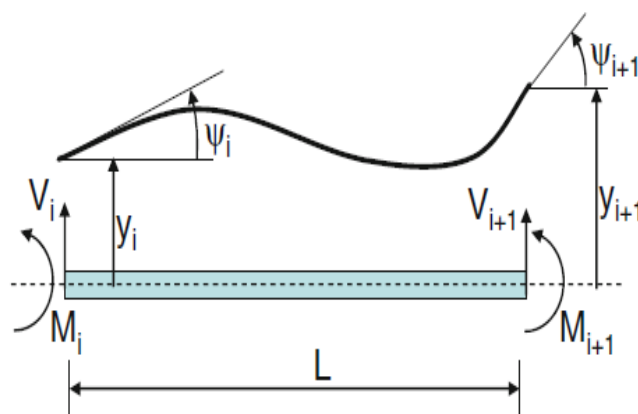


Fig. 2 Turbine Blade with space reticulation (a), Dynamic model of blade (b)

In a bond graph formulation, the potential energy storage is represented as a four-port C-field. The i^{th} beam element is influenced by displacements y_i and y_{i+1} , and rotations ψ_i and ψ_{i+1} . The flow variables in four ports of the C-field are the corresponding linear and rotational velocities. The effort variables are the shear

forces and bending moments. The stiffness of the beam element relates these generalized Newtonian forces to the generalized displacements at the ends of the element as (1), (2) and (3).

$$\begin{bmatrix} F_{yi} \\ M_{zi} \\ F_{yi+1} \\ M_{zi+1} \end{bmatrix} = [K_{fyi}] \begin{bmatrix} y_i \\ \psi_{zi} \\ y_{i+1} \\ \psi_{zi+1} \end{bmatrix} \tag{1}$$

$$\begin{bmatrix} F_{zi} \\ M_{yi} \\ F_{zi+1} \\ M_{yi+1} \end{bmatrix} = [K_{fzi}] \begin{bmatrix} y_i \\ \psi_{yi} \\ y_{i+1} \\ \psi_{yi+1} \end{bmatrix} \tag{2}$$

$$\begin{bmatrix} M_{xi} \\ M_{xi+1} \end{bmatrix} = [K_t] \begin{bmatrix} \psi_{xi} \\ \psi_{xi+1} \end{bmatrix} \tag{3}$$

Where $[K_{fyi}]$ is the flexural stiffness around y , $[K_{fzi}]$ is the flexural stiffness around z and, $[K_t]$ is the flexural stiffness

$$[K_{fyi}] = \frac{E(I_{zi-1} + I_{zi})}{\left(l_{i-1} + \frac{l_i}{2}\right)^3} \begin{bmatrix} 12 & 6(l_{i-1} + l_i/2) & -12 & 6(l_{i-1} + l_i/2) \\ 6(l_{i-1} + l_i/2) & 4(l_{i-1} + l_i/2)^2 & -6(l_{i-1} + l_i/2) & 2(l_{i-1} + l_i/2)^2 \\ -12 & -6(l_{i-1} + l_i/2) & 12 & -6(l_{i-1} + l_i/2) \\ 6(l_{i-1} + l_i/2) & 2(l_{i-1} + l_i/2)^2 & -6(l_{i-1} + l_i/2) & 4(l_{i-1} + l_i/2)^2 \end{bmatrix} \tag{1}$$

$$[K_{fzi}] = \frac{E(I_{yi-1} + I_{yi})}{\left(l_{i-1} + \frac{l_i}{2}\right)^3} \begin{bmatrix} 12 & -6(l_{i-1} + l_i/2) & -12 & -6(l_{i-1} + l_i/2) \\ -6(l_{i-1} + l_i/2) & 4(l_{i-1} + l_i/2)^2 & 6(l_{i-1} + l_i/2) & 2(l_{i-1} + l_i/2)^2 \\ -12 & 6(l_{i-1} + l_i/2) & 12 & 6(l_{i-1} + l_i/2) \\ -6(l_{i-1} + l_i/2) & 2(l_{i-1} + l_i/2)^2 & 6(l_{i-1} + l_i/2) & 4(l_{i-1} + l_i/2)^2 \end{bmatrix} \tag{2}$$

$$[K_t] = \frac{GJ}{L} \begin{bmatrix} 1 & -1 \\ -1 & 1 \end{bmatrix} \tag{3}$$

Where E is the Young module of the material, G is the Coulomb module, $I_{y,z}$ the second moments of area about the axis of deflection, J is the second polar moment and L is the length of the finite element, Note that the stiffness matrix is symmetric. This stiffness matrix is derived by taking partial derivatives of the strain energy with respect to the individual nodal displacements. The structural damping matrix is given by $[R_i]=\mu[K_i]$, where the μ factor represents the coefficient of structural damping.

The Bond Graph representation of the combined stiffness and damping of the beam element is then given as shown in Fig. 3.

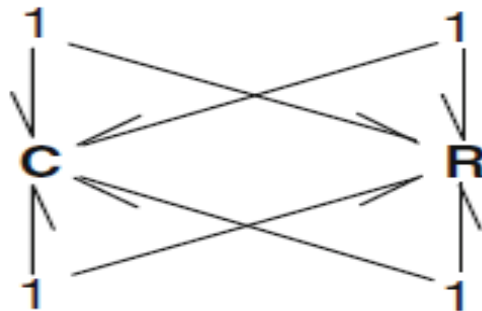


Fig. 3 Representation of element stiffness and damping in Rayleigh beam Bond Graph model

Fig. 4 shows the Bond Graph model of the blade. Fig. 4(a) represents the axial extension deformation of the blade, Fig. 4(b) the tangential extension deformation and Fig. 4(c) the torsional deformation of blade. For Fig. 4(a) and Fig. 4(b), two motions are shown: rotation at the top and translation at the bottom of the figure. In Fig. 4(c) the model is represented by one rotation motion. For each model, the displacements and rotations at the center of gravity of each element are represented by 1-junction. For each element aerodynamic forces are applied, meanings that the effort is imposed. The stiffness and the structural damping matrixes between the centers of gravity of adjacent elements are represented using C-field and R-field elements, respectively.

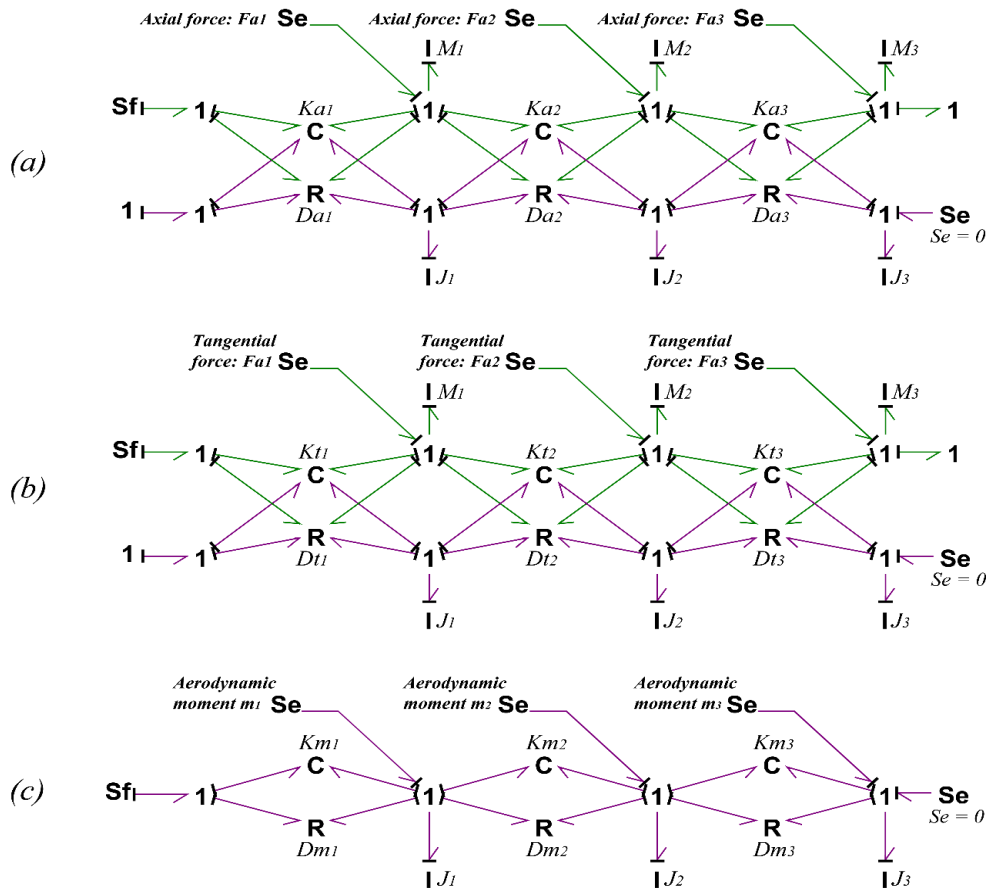


Fig. 4 Structural bond graph of blade, axial extension (a), tangential extension (b), torsional extension (c)

Boundary conditions of the model for the tangential extension deformation are represented by the Sf and Se sources. Connection between the blade and the hub must be rigid, i.e. $Sf = 0$, and the blade has only one degree of freedom, so $Se = 0$. Boundary conditions for the axial extension deformation are represented by the Se source. The blade has only one degree of freedom, then $Se = 0$. Connection between the blade and the hub as well as between the hub and the tower are assumed to be rigid. Therefore, the movement at the tower top is the same as the movement at the blades bottom. This relationship between the blade and the tower can be modeled by I -junction. Boundary conditions for the torsional deformation are represented by the Sf source which represents the pitch actuator system's velocity. Dynamic equations and natural frequencies of the blade can be directly obtained from the Bond Graph model.

Three sources of effort, which represent the aerodynamic forces, need to be calculated in the input wind. This process will be treated in the aerodynamic subsystem section. Sub-models, as shown in Fig. 5 can represent the model of the blade (Fig. 4).

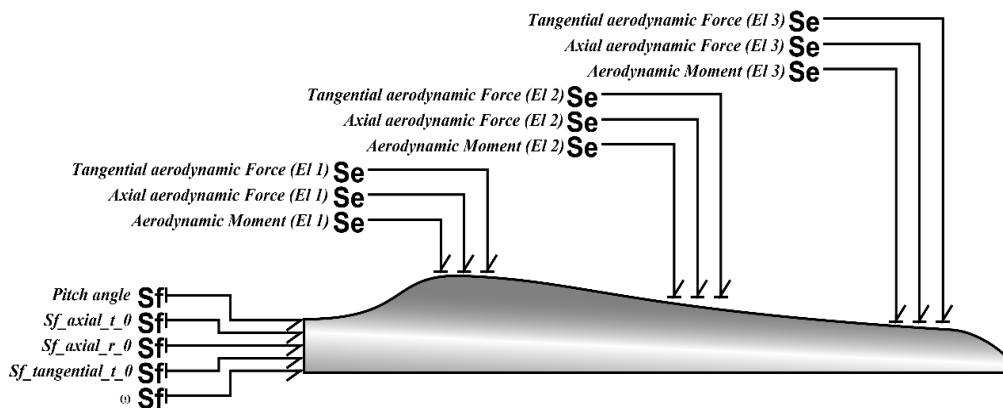


Fig. 5 Tree sections bond graph blade
III. Aerodynamic Subsystem

The aerodynamic subsystem transforms the three-dimensional wind field into lumped forces acting on the rotor blades. The inputs to the aerodynamic subsystem are the wind speed V , the pitch angle β , the rotational and axial speeds of the rotor ω and the axial displacement of the blades caused by flapping and tower bending y_b , respectively. Its outputs are the aerodynamic torque T_r , tangential force F_r , the thrust force F_T and the aerodynamic moment.

Wind turbine aerodynamic models are used to relate wind inflow conditions to the loads applied to the turbine. The subsequent analysis develops the most common aerodynamics theory employed in the wind turbine design and analysis environment. It corresponds to the Blade Element Momentum theory (BEM). Extensive literature deals with the BEM theory explanation and presentation [15,16]. The BEM Theory combines two methods of examining how a wind turbine operates. The first method uses a momentum balance on a rotating annular stream tube passing through a turbine. Axial Thrust dF_T and Tangential Force dF_r -in terms of flow parameters, are:

$$dF_T = 4a(1 - a)\rho V^2 \pi r dr \tag{74}$$

$$dF_r = 4a'(1 - a)\rho V \Omega_r \pi r^2 dr \tag{85}$$

Where V represents the wind velocity, ρ the air density, a the axial induction factor, a' the angular induction factor, ω the angular velocity of the blades, and r is the radius of an annular element, having a thickness dr .

The second method is to examine the forces generated by the airfoil lift and drag coefficients at various sections along the blade. Axial Force, Tangential Force and Aerodynamic Moment - in terms of the lift, the drag and the pitching moment coefficients of the airfoil, are as follows:

$$dF_T = \frac{1}{2} \rho \frac{V^2(1 - a)^2}{\sin^2 \phi} (C_L \cos \phi + C_D \sin \phi) c dr \tag{9}$$

$$dF_r = \frac{1}{2} \rho \frac{V^2(1 - a)^2}{\sin^2 \phi} (C_L \sin \phi - C_D \cos \phi) c dr \tag{106}$$

$$dM_x = \frac{1}{2} \rho \frac{V^2(1 - a)^2}{\sin^2 \phi} [C_m c + y_G (C_L \cos \phi + C_D \sin \phi) - (z_G - z_a) (C_L \sin \phi - C_D \cos \phi)] c dr \tag{11}$$

$$\phi = \tan^{-1} \left(\frac{V(1 - a)}{\Omega_r r (1 + a')} \right) \tag{12}$$

Where c is the chord length of the blade element, the wind inflow angle, ϕ is the angle between the local flow direction and the rotor plane (Equation 12), parameters involved in these expressions are graphically represented in Fig.6(a). (y_G, z_G) are the center of gravity coordinates, z_a : the aerodynamic center's coordinate, as shown in Fig. 6(b).

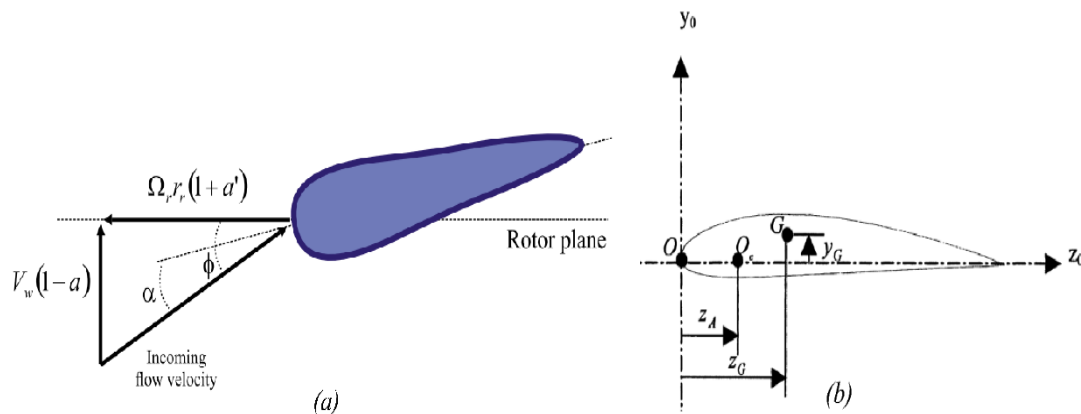


Fig. 6 Velocities at rotor plane (a), Center of gravity coordinates and the aerodynamic center (b)

C_L , C_D and C_m are lift, drag and pitching moment dimensionless coefficients respectively as functions of the angle of attack α . Lift, Drag and Pitching moment coefficients for a NACA 4415 airfoil are shown in Fig 7. This graph indicates that for low values of incidence angle, the airfoil successfully produces a large amount of lift with little drag.

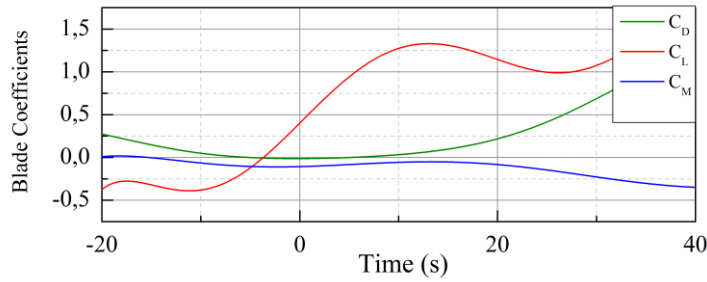


Fig.7 Lift, Drag and pitching moment Coefficients for a NACA

Equations (7) and (9) are used to calculate the axial induction:

$$a = \left(1 + \frac{4\sin^2\phi}{\sigma'(C_L\cos\phi + C_D\sin\phi)}\right)^{-1} \tag{13}$$

Equations (8) and (10) are used to calculate the tangential induction factor:

$$a' = \left(-1 + \frac{4\sin\phi\cos\phi}{\sigma'(C_L\sin\phi - C_D\cos\phi)}\right)^{-1} \tag{14}$$

Solution for a given blade cannot be found directly from the equations but an iterative method is required to calculate the axial induction factor, the tangential induction factor, angles of attack and thrust coefficients for each section along the span of the blade. It is composed of the following steps:

1. Estimate the initial value of the axial induction factor a_i and the tangential induction a'_i relative to the i^{th} blade element.

An efficient technique (among others) is to assume that the inflow angle is small: $\sin\phi_i \approx \phi_i$. The tangential induction a'_i and the drag coefficient C_{Di} are null. The lift coefficient is $C_{Li} = 2\pi\alpha_i$, where the angle of attack is $\alpha_i = \phi_i - \beta_i$, with β_i the sum of the twist angle β_i depending on the position of the center of gravity of the i^{th} section and the pitch angle β which is an input control variable.

After some rearranging, it yields to:

$$a_i = \frac{1}{4} \left(2 + \pi\lambda_{ri}\sigma'_i - \sqrt{4 - 4\pi\lambda_{ri}\sigma'_i + \pi\lambda_{ri}^2\sigma'_i(8\beta_i + \pi\sigma'_i)}\right) \tag{157}$$

With: $\lambda_{ri} = \frac{\Omega r_i}{V}$ is the local speed ratio and $\sigma'_i = \frac{c_i}{2\pi r_i}$ is the local solidity, calculated using chord values c_i depending on r_i (Appendix A).

2. Use the initial value of a_i and a'_i to calculate ϕ_i .

$$\phi_i = \tan^{-1}\left(\frac{V(1 - a_i)}{\Omega r_i(1 + a'_i)}\right) \tag{168}$$

3. Calculate incidence angle α_i and then C_{Li} and C_{Di} using look-up tables (Fig 20)

$$\alpha_i = \phi_i - \beta_i \tag{179}$$

4. Calculate new values of a_i and a'_i using the following Equations :

$$a_i = \left(1 + \frac{4\sin^2\phi_i}{\sigma'_i(C_{Li}\cos\phi_i + C_{Di}\sin\phi_i)}\right)^{-1} \tag{18}$$

$$a'_i = \left(-1 + \frac{4\sin\phi_i\cos\phi_i}{\sigma'_i(C_{Li}\sin\phi_i - C_{Di}\cos\phi_i)}\right)^{-1} \tag{19}$$

In this process iterations are done until the values of induction factors and inflow angle converge to their final values, and then we can calculate the axial force and the tangential force for each section along the blade by:

$$F_{Ti} = \frac{1}{2}\rho \frac{V^2(1 - a_i)^2}{\sin^2\phi_i} (C_{Li}\cos\phi_i + C_{Di}\sin\phi_i)c_i l_i \tag{20}$$

$$F_{ri} = \frac{1}{2}\rho \frac{V^2(1 - a_i)^2}{\sin^2\phi_i} (C_{Li}\sin\phi_i - C_{Di}\cos\phi_i)c_i l_i \tag{21}$$

$$M_{xi} = \frac{1}{2} \rho \frac{V^2 (1 - a_i)^2}{\sin^2 \phi_i} [C_{mi} c_i + y_{Gi} (C_{Li} \cos \phi_i + C_{Di} \sin \phi_i) - (z_{Gi} - z_{ai}) (C_{Li} \sin \phi_i - C_{Di} \cos \phi_i)] c_i l_i \tag{22}$$

The fundamental aerodynamic theory used by the bond graph model is presented in this paper. A MGY-element of bond graph is used to implement equations (15) through (22), with wind flow (MSf source) being transformed into aerodynamic forces (Se source), as shown in Fig. 8.

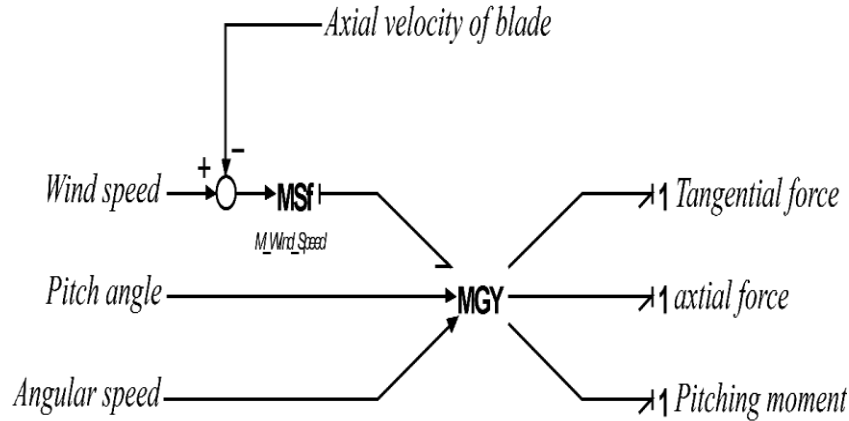


Fig. 8 Bond graph model of the aerodynamic subsystem

Modulated inputs to MGY elements of Fig. 8 are the pitch angle β , the angular velocity Ω_r , and the wind speed V and the axial displacement of the blades caused by flapping and tower bending. In order to simulate the blade model, equations (15) through (22) are integrated within each MGY element; which means that their traditionally constitutive relation is changed.

IV. Simulation And Results

To validate the Bond Graph model, a simulation of the power coefficient C_p is done. This parameter characterizes wind turbines. It represents the fraction of the power extracted on the turbine from the available power in the wind. It can be written as:

$$C_p = 4a(1 - a)^2 \tag{10}$$

The theoretical maximum power coefficient from an idealized rotor C_{pmax} , known as Betz limit, can be found by setting the derivative of C_p with respect to a equal to zero, which leads to : $a=1/3$ and $5 C_{pmax} = 0.596$ which corresponds to the maximum possible efficiency for an idealized wind turbine of 59.6%.

To make this simulation, we connect the MGY elements with the blade as shown in Fig. 9. Then we set the wind speed to a constant value equal to $12m/s$, then we apply a slope ramp equal to 1 for the speed and we simulate the model for three values of β (2, 4 and 6). Finally we compute C_p by Equation 24 and then we show the results of C_p as a function of the tip speed λ ($\lambda=R\omega/V$) as shown in Fig.10.

$$C_p = \frac{3T_r \Omega_r}{\frac{1}{2} \rho \pi R^2 V^3} \tag{24}$$

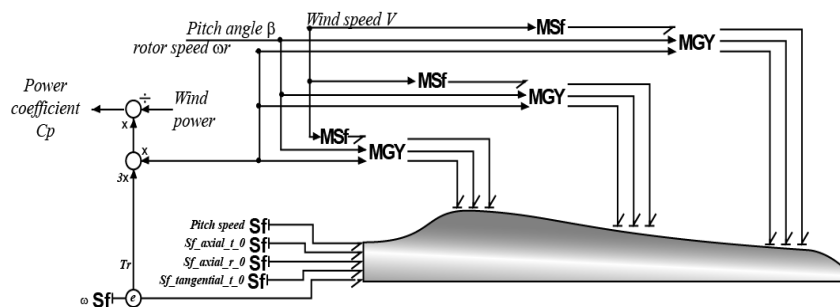


Fig. 9 Simulation model of wind turbine blade

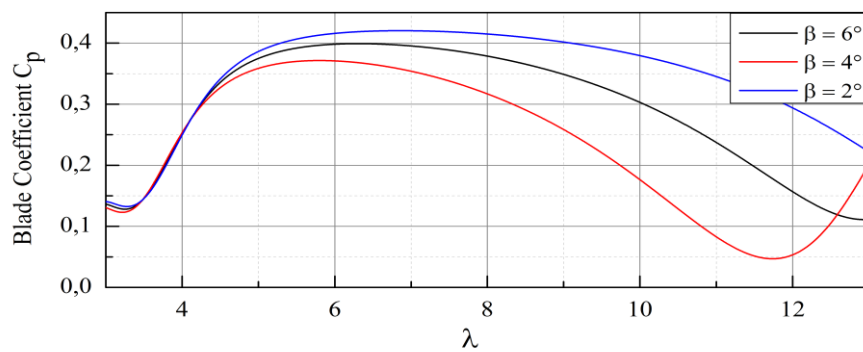


Fig. 10 Curve of C_p vs λ

From the figure the maximum values of C_p is 0.42, having a tip speed of 7; the theoretical maximum value of C_p is 0.596, known as Betz limit, at around a tip speed of 7. In practical designs, the maximum achievable C_p is below 0.5. The difference to standard values is acceptable and it is better that the value shown in [14] (around 0.33). This simulation confirms that dynamical model of the blade bearing adequately performs.

V. Conclusion

Due to interactions between aerodynamic, mechanical subsystems, a dynamic model of a wind turbine generating system using the Bond Graph Approach is proposed to analyze the dynamic behavior of a wind turbine blade. It consists in considering the blade as a Rayleigh beam composed of a number of sections submitted to aerodynamic forces calculated using the BEM theory. The value of power coefficient curve indicates the validity of the proposed Bond Graph model of wind turbine. The model has been validated with the available data (NACA 4415), but the proposed blade model is a generic model and can be used with any profile of blade. Power Coefficient curve can be predicted and hence the optimum conditions to operate.

References

- [1]. Ahlstrom A. Influence of wind turbine flexibility on loads and power production. *Wind Energy* 2006;9(3):237-49
- [2]. I. Chopra, J. Dugundji, Non-linear dynamic response of a wind turbine blade, *J. Sound Vib.* 63 (2) (1979) 265–286
- [3]. D. Lee, D.H. Hodges, M.J. Patil, Multi-flexible-body dynamic analysis of horizontal axis wind turbines, *Wind Energy* 5 (4) (2002) 281–300.
- [4]. A. Baumgart, A mathematical model for wind turbine blades, *J. Sound Vib.* 251 (1) (2002) 1–12.
- [5]. J.W. Larsen, S.R.K. Nielsen, Non-linear dynamics of wind turbine wings, *Int. J. Nonlinear Mech.* 41 (5) (2006) 629–643.
- [6]. J.W. Larsen, S.R.K. Nielsen, Nonlinear parametric instability of wind turbine wings, *J. Sound Vib.* 299 (1–2) (2007) 64–82.
- [7]. J.W. Larsen, R. Iwankiewicz, S.R.K. Nielsen, Nonlinear stochastic stability analysis of wind turbine wings by Monte Carlo simulations, *Probab. Eng. Mech.* 22 (2) (2007) 181–193.
- [8]. H. Arvin, W. Lacarbonara, F. Bakhtiari-Nejad, A geometrically exact approach to the overall dynamics of elastic rotating blades – Part 2: flapping nonlinear normal modes, *Nonlinear Dyn.* 70 (3) (2012) 2279–2301.
- [9]. V. Ramakrishnan, B.F. Feeny, In-plane nonlinear dynamics of wind turbine blades, in: *Proceedings of the ASME 2011 International Design Engineering Technical Conferences & Computers and Information in Engineering Conference*, Washington, DC, USA, August 28–31, 2011.
- [10]. Zakaria Khaouch, Mustapha Zekraoui, JamaaBengourram, Nourreddine Kouider, Mustapha Mabrouki. *Mechatronic modeling of a 750 kW fixed-speed wind energy conversion system using the Bond Graph Approach.* *ISA Transactions* 65 (2016) 418-436.
- [11]. Zakaria Khaouch, Mustapha Zekraoui, Nourreddine Kouider, Mustapha Mabrouki, JamaaBengourram. *Mechatronic Modeling and Control of a Nonlinear Variable-Speed Variable-Pitch Wind Turbine by Using the Bond Graph Approach.* *IOSR Journal of Electrical and Electronics Engineering (IOSR-JEEE)*. e-ISSN: 2278-1676,p-ISSN: 2320-3331, Volume 11, Issue 6 Ver. I (Nov. - Dec. 2016), PP 95-115
- [12]. Margolis Donald. *Bond Graph Modelling of Engineering Systems: Theory, Applications and Software Support*; 2011.
- [13]. MerzoukiRochdi, SamantarayArun Kumar, Pathak Pushparaj Mani, OuldBouamamaBelkacem. *Intelligent mechatronic systems: modeling, control and diagnosis.* 2013.
- [14]. Agarwal S, Chalal L, Dauphin-Tanguy G, Guillaud X. *Bond graph model of wind turbine blade.* In: *Bond graph model: theory and Practice.* Vienna: MathMod; 2012.
- [15]. Liu Xiong, Chen Yan, Ye Zhiqun. *Wind turbine computing model of aerodynamic performance with horizontal axis.* *J Sol Beijing* 2005;26:792–800.
- [16]. Hansen MOL, Sorensen JN, Voutsinas S, Sorensen N, Madsen HA. *State of the art in wind turbine aerodynamics and aeroelasticity.* *Progress AerospSci* 2006;42:285–330.

Zakaria Khaouch" Dynamic Study of A Wind Turbine Blade Using Bond Graph." *IOSR Journal of Mechanical and Civil Engineering (IOSR-JMCE)* , vol. 14, no. 6, 2017, pp. 55-63.